Miner Deposita (2006) 41: 339–355
DOI 10.1007/s00126-006-0063-9

ARTICLE

M. Eugenia Cisternas · Juan Hermosilla

The role of bitumen in strata-bound copper deposit formation in the Copiapo area, Northern Chile

Received: 22 January 2004 / Accepted: 11 April 2006 / Published online: 7 June 2006

Abstract In northern Chile, between 27 and 33°S, there are numerous deposits where residual petroleum is associated with Cu-(Ag) mineralisation (the most famous being El Soldado). All of these deposits are hosted by Lower Cretaceous volcanic or volcanoclastic facies along the axis of a former backarc basin. This close relationship suggests that the generation, migration and emplacement of hydrocarbons in the Cretaceous volcanic units is a regional process, associated with the evolution of the Cretaceous backarc basin and points to the importance of pyrobitumen as an exploration tool for similar Cu–(Ag) deposits. The present work analyses four small strata-bound copper deposits located along a north–south belt approximately 10 km east of Copiapó in northern Chile. These deposits are typically hosted by pyrobitumen-rich andesitic volcanic to volcanoclastic rocks intercalated with the marine carbonate Pabellón Formation, the youngest formation within the Chañarcillo Group. The strong genetic and spatial relationships between the pyrobitumen-rich lavas and the mineral deposits allow us to define this volcanic belt as the Ocoita-Pabellón Metallotect. Two hydrothermal events can be distinguished based on the mineralogical, textural, fluid inclusion and isotope data of ore and gangue and on the optical properties of residual petroleum. During the early event, petroleum was mobilised from the source rocks into the primary and secondary porosity of the lavas by Fe-rich hydrothermal fluids, which precipitated pyrite as an early sulphide phase. The second event is characterised by Cu-rich hydrothermal fluids, which induced three successive sub-stages of Cu-sulphide precipitation. The hydrothermal fluids chemically and thermally altered the first-stage bitumen, transforming it into pyrobitumen. The present work documents similarities between the Ocoita-Pabellón Metallotect and the El Soldado ore deposit and emphasises important differences. In the El Soldado host rocks, a petroleum reservoir existed prior to the arrival of the mineralising hydrothermal fluids, the framboidal pyrite was formed by assistance of bacteria, the S of the Cu sulphides was inherited from the pyrite, and the fluid source was basin connate-metamorphic brine. In the Ocoita-Pabellón Metallotect, the hydrocarbons were mobilised into the host rocks by hydrothermal fluids; the pyrite is epigenetic, the $\delta^{34}S$ values of pyrite and copper sulphides are very different, with distinctive light $\delta^{34}S$ signature of Cu sulphides ($\delta^{34}S$ between −44.7 and −17.9‰), and the calculated $\delta^{18}O$ of hydrothermal fluids indicates the participation of meteoric water in the late phases of the hydrothermal system.

Keywords Strata-bound Cu deposits · Pyrobitumen · Stable isotopes · Volcanic-hosted · Early Cretaceous · Chile

Editorial handling: G. Beaudoin

M. E. Cisternas (✉)
Instituto de Geología Económica Aplicada (GEA),
Universidad de Concepción,
Concepción, Chile
e-mail: mcistern@udec.cl
Fax: +56-41-242535

J. Hermosilla
SKM Minmetal Ltda.,
Av. José Domingo Cañas 2681, Ñuñoa,
Santiago, Chile
e-mail: jherm001@codelco.cl

Introduction

Strata-bound mineral deposits hosted in solid hydrocarbon-bearing Cretaceous sequences deposited in an extensional basin are common in central Chile. The association of mineralisation and migrated hydrocarbon hosted in lavas, sub-volcanic intrusive and pyroclastic rocks of the Cretaceous backarc basin of central Chile has been reported at one of the largest manto-type deposits of Chile: El Soldado (32° 38′ S) (see Wilson 1998, 2000; Wilson and Zentilli 1999; Boric et al. 2002; Wilson et al. 2003a,b). Other related deposits occur at La Serena: (see Zentilli et al. 1994; Wilson 1998; Cucurella et al. 2005; Wilson and Zentilli 2006) and Copiapó (see Cisternas and Frutos 1996; Cisternas et al. 1999a,b; Hermosilla 2001; Haggan et al. 2003).

In the Copiapó area of northern Chile, in a geological framework similar to that of El Soldado and Talcuna, there is a group of small manto-type deposits hosted by solid hydrocarbon-rich lavas and volcanic rocks of Lower Cretaceous age (Fig. 1). In general, these deposits show notable similarities with El Soldado: the same age for the host rocks and the same type of hydrothermal alteration stages (an early Fe-rich stage associated with the migration and emplacement of oil, followed by a late, Cu-rich event). However, the present study also demonstrates that there are important differences, such as in the Copiapó area, the migration of hydrocarbons occurred together with the Fe-rich hydrothermal fluids.

During the early evolution of the Cretaceous backarc basin in Chile, organic-rich sequences were deposited both in central (El Soldado area: see Boric et al. 2002) and northern Chile (Copiapó area: see Cisternas and Diaz 1990). The subsequent thermal evolution of these sequences during burial would have generated the hydrocarbons. The regional heating (increased with the extension and thinning of the crust under the backarc basin) contributed to the thermal maturation and cracking of the migrated oil to form pyrobitumen. Hydrothermal fluid circulation (associated with active magmatism during the Early and Late Cretaceous) could have removed the

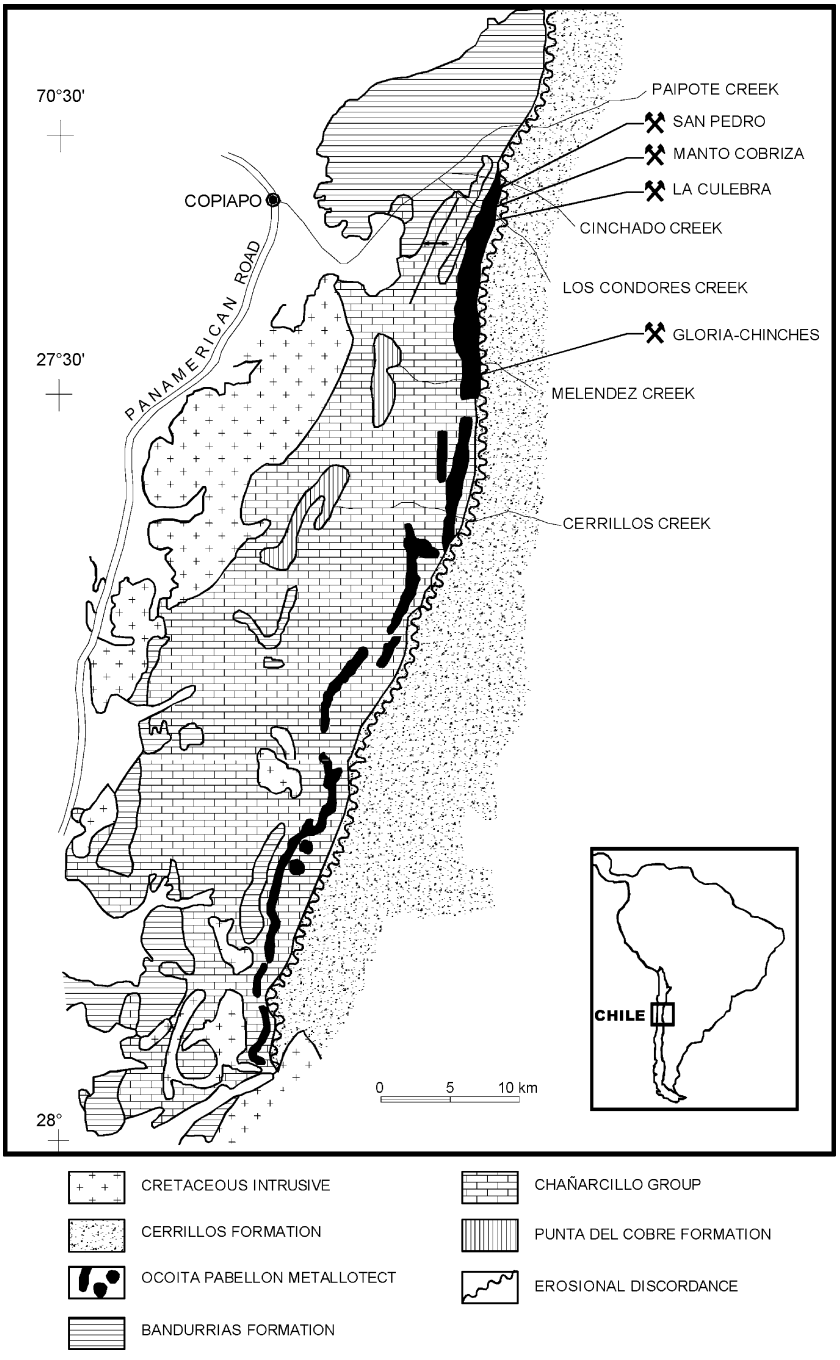

Fig. 1 Geologic map of Cretaceous units around Copiapó (modified from Segerstrom 1968)

hydrocarbons from their source rocks and deposited them in the upper levels of the Lower Cretaceous sequence.

The present study is a combined investigation of solid hydrocarbon properties and their paragenetic relationships with mineralisation and gangue. We present reflectance and anisotropy data of solid hydrocarbons (bitumen and pyrobitumen), $\delta^{13}C$ values of pyrobitumen and hydrothermal calcite, $\delta^{34}S$ values of the Fe- and Cu-sulphides stages, thermometric data of fluids trapped in the successive generations of hydrothermal calcite and $\delta^{18}O$ values of the late calcites.

The principle objective of this study has been to investigate (1) the thermal history of the mineral deposits by characterising the thermal maturity of the solid hydrocarbons and (2) the hydrothermal fluids involved to gain insight into the role of pyrobitumen in the hydrothermal processes.

Field and analytical methods

Samples containing solid hydrocarbons and mineralisation were selected from surface outcrops or underground works for each deposit. To separate minerals and solid hydrocarbons, the samples were crushed and the phases of interest were handpicked.

The mineralogy, textural and paragenetic relationships of 25 polished thin sections from the deposits were studied using a petrographic microscope. The samples for fluid inclusion and isotope studies were carefully selected to represent the different paragenetic stages.

Solid hydrocarbon samples were mounted and polished using standard coal preparation techniques as described by Bustin et al. (1985). Random reflectance (R_0, without polariser) was performed on 34 polished samples under immersion oil using a Leitz MPV-Combi microscope at 546 nm. For each sample, 25 to 30 reflectance measurements were taken.

Thermometric data in seven samples from the four studied deposits were collected using a model TP-92 Linkman heating/freezing stage. Fluid salinity, expressed as weight percent NaCl equivalent (wt. % NaCl eq.), was determined according to the method of Potter et al. (1978).

S (on sulphide concentrates), C and O (on calcite) isotope analyses were carried out at the Natural Environment Research Council Isotope Geosciences Laboratory (Keyworth, UK). For S, the results are expressed as per mil deviations from the Vienna Canyon Diablo Troilite (V-CDT) reference material with an analytical reproducibility of ±0.1‰. For C and O, the results are expressed as per mil deviations from the Vienna Peedee Belemnite (V-PDB) and from the Vienna Standard Mean Ocean Water (V-SMOW) reference materials, with analytical reproducibility better than ±0.05‰.

Geological setting

During the Late Jurassic–Early Cretaceous, the western side of South America was an active margin, characterised by a magmatic backarc basin complex formed as a result of eastward subduction of the oceanic lithosphere under South America. In Peru and southernmost Chile (region of Magallanes), the extensional event formed marginal basins (with oceanic crust construction), while in northern and central Chile (Fig. 2), the extensional process, aborted before oceanic crust construction, favoured volcanic rock extrusions in troughs developed in continental crust (Aberg et al. 1984; Mpodozis and Ramos 1990), such as the

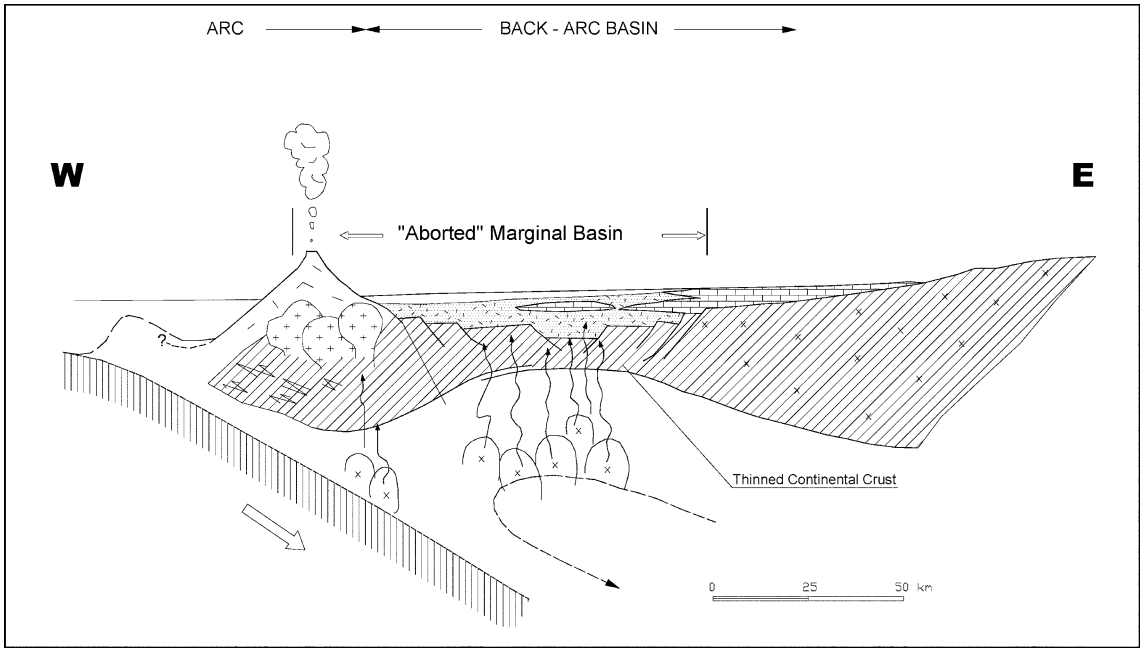

Fig. 2 Lower Cretaceous tectonic setting at the Copiapó latitude (modified from Mpodozis and Ramos 1990)

Aconcagua Basin in central Chile (33°S) and its northern extension, the Atacama Basin in the Copiapó area (27°S).

The aborted, marginal Atacama Basin is filled with 1,700 to 2,000 m of Upper Valanginian to Aptian carbonate facies (Chañarcillo Group) accumulated under shallow marine conditions (Figs. 1 and 3). The Chañarcillo Group (Segerstrom 1960; Cisternas and Diaz 1990; Marschik and Fontboté 2001) is composed of four formations (from bottom to top): (1) the Abundancia Formation (Late Valanginian), a 200-m-thick unit of bedded limestone and chert with intercalations of volcanic arenite, tuff and volcaniclastic breccias; (2) the Nantoco Formation (Early Hauterivian), a 800- to 1,200-m-thick sequence of limestone, calcareous shale, mudstone and bituminous limestone; (3) the Totoralillo Formation (Late Hauterivian), consisting of alternating limy shale and bio-clastic limestone with a thickness ranging from a maximum of 225 m at Meléndez Creek, to 75 m between the Cinchado and Los Cóndores creeks towards the north; (4) the Pabellón Formation (Barremian-Aptian), a 433-m-thick unit composed of a sandy calcareous sequence with minor bio-extraclastic calcilutites and laminated mudstones, capped by porphyritic lavas (locally named "ocoitic lavas") and small, irregular lenses of lithic tuffs (Cisternas et al. 1999a). For a long time, the porphyritic rocks were considered to be a sill (Segerstrom 1960; Arévalo 1994, 1995), until Cisternas et al. (1999a,b) demonstrated their volcanic origin. The lavas and tuffs of the Pabellón Formation are the host rocks of the mineral deposits studied here (Fig. 1).

The magmatic system of the Lower Cretaceous backarc complex is represented in the Copiapó area (Fig. 1) by intrusive and volcanic–volcanoclastic units. The intrusive rocks, cropping out south of Copiapó, are part of the Coastal Batholith of northern Chile and consist mainly of calc-alkaline, medium- to coarse-grained diorite, granodiorite, tonalite, monzodiorite and quartz monzodiorite (Marschik et al. 2003). The ages of these rocks range from 119 to 97 Ma (Arévalo 1994, 1995, 1999; Ullrich et al. 2001).

The volcanic and volcanoclastic rocks range from mainly andesitic (locally dacitic) to basalt andesitic flows and breccias. They are known in the Copiapó area as the Punta del Cobre and Bandurrias formations. According to Marschik and Fontboté (2001), both units have similar lithologies and show a similar range of geochemical compositions and petrographic–volcanic affinities. For these reasons, these authors suggest the inclusion of both units in the Bandurrias Group. The only distinction that can be made between the Punta del Cobre Formation and the Bandurrias Formation is based on their stratigraphic positions relative to the Chañarcillo Group (Fig. 3). The Punta del Cobre Formation underlies the Chañarcillo Group carbonate facies formations, whereas the Bandurrias Formation interfingers to the north and east with the marine backarc basin units (Chañarcillo Group), and therefore represents the terrestrial time-equivalent of the marine environments (Fig. 3).

During the late Aptian period, marine conditions ceased and the Atacama Basin was filled by a 4,500-m-thick sequence of continental conglomerates, sandstones and lavas, locally referred to as the Cerrillos Formation (Figs. 1 and 3). During the early late Cretaceous period, a transpressional phase, related to the opening of the South Atlantic Ocean and the rapid spreading in the southeast Pacific ridge (Larson and Pitman 1972; Vaughan 1995), initiated the inversion of the Atacama Basin.

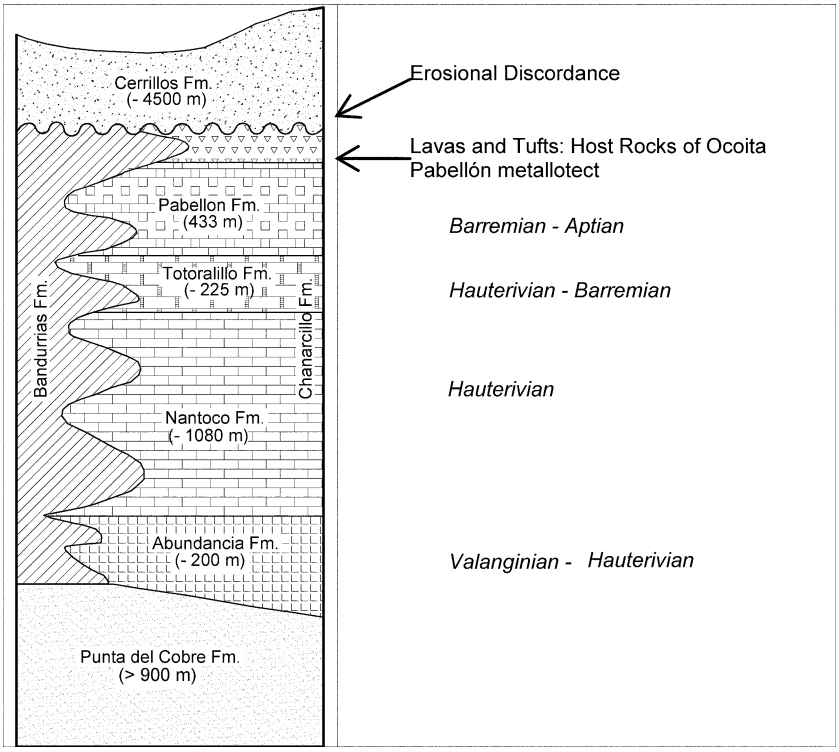

Fig. 3 Stratigraphic relationships of the Lower Cretaceous units in the Copiapó area (from Marschik and Fontboté 2001)

The solid hydrocarbon, Cu(Fe)-sulphide-bearing deposits in Copiapó

Cisternas and Frutos (1996) presented the first documentation of a marked spatial relationship between migrated solid hydrocarbons within a narrow belt of porphyritic lavas (upper part of the Pabellón Formation) in the Copiapó Region. This volcanic belt, which extends for almost 70 km along the axis of the Lower Cretaceous Atacama Basin, has a thickness range from 200 to 300 m in Carrizalillo Creek, and is absent north of Los Cóndores Creek (Fig. 1). The occurrence of a number of small manto-type mineral deposits hosted in this volcanic belt, where residual petroleum is associated with Cu(Ag) mineralisation, was the basis used to define these mappable geological features as the "Ocoita-Pabellón Metallotect" (Cisternas and Frutos 1996; Cisternas et al. 1999a) in the Copiapó Region. The present work analyses four of these manto-type deposits located approximately 10 km east of Copiapó, between the Cinchado (27°22′ S) and Meléndez (27°29′ S) creeks. From north to south, the deposits are (see Fig. 1): San Pedro (2.0% Cu; 21 ppm Ag), Manto Cobriza (4.3% Cu; 48 ppm Au), La Culebra (3.5% Cu) and Gloria-Chinches (2.5% Cu; 30 ppm Ag). Most of the deposits are represented by abandoned underground mines. In some, small-scale exploitations (30–130 ton/month) are still being performed.

The host rocks of the studied deposits are porphyritic lavas and tuffs located in the volcanic upper part of the marine Pabellón Formation. According to Cisternas et al. (1999a), the lavas and tuffs are andesite and pyroxene-bearing andesite, similar to the lavas from the Ocoa member of the Veta Negra Formation (Thomas 1958) of central Chile, where they are named "ocoitas" or "ocoitic lavas". Texturally, the lavas display porphyritic and vesicular textures, with phenocrysts (25–40 vol%) of centimeter-size plagioclase (strongly altered labradorite), pyroxene, relicts of olivine and primary magnetite. The vesicles are filled with calcite, quartz, K-feldspar, chlorite, solid hydrocarbons and copper sulphides in mineralised areas. The groundmass is generally composed of plagioclase-microliths with interstitial pyroxene, sphene, magnetite and rutile as accessory minerals; in some cases, the groundmass is composed of strongly devitrified glass. The average silica content is 54.3%. Based on immobile trace element analyses, Cisternas et al. (1999a) concluded that the lavas were erupted from high K-calcalkaline and transitional magmas in an active continental margin having a strong intra-plate component. The extrusion of the lavas and tuffs was controlled by structures associated with continental crust spreading and thinning in the backarc region, similar to the process that controlled the fissural extrusion of Lower Cretaceous lavas in central Chile (Veta Negra Formation, Vergara and Nystrom 1996).

In mineralised areas, the volcanic host rocks display moderate to strong propylitic hydrothermal alteration. Locally, silicification and calcification are strong. Alteration occurs both as veinlets and as mineral replacements, and calcite veinlets commonly produce a micro-breccia texture. Zeolites and hydrothermal chlorite intergrowths with copper sulphides are common. Pervasive alteration by potassic feldspar, albite and epidote is also common (Hermosilla 2001).

Ore mineralogy and paragenesis

Textural and paragenetic studies of polished thin sections from the four studied deposits of the Copiapó area (Fig. 1) demonstrate the existence of four principle mineral associations, which characterise two distinct hydrothermal events.

Early Fe-rich hydrothermal event

Fe-sulphide stage The early Fe-rich hydrothermal event is characterised by the paragenetic association of Fe sulphides (pyrite and scarce marcasite), chlorite, calcite I and bitumen[1] (R_0<0.7%; Table 1) filling vesicles and veinlets. Bitumen and the hydrothermal minerals show intergrown textures or sequential textures (Figs. 4a,b and 5a), suggesting that the hydrocarbons were transported into the primary and secondary porosity of the lavas by the hydrothermal Fe-rich fluids. Calcite II occurs as veinlets cutting the iron-sulphide mineral stage (Fig. 5b).

Late Cu-rich hydrothermal event

The second event is characterised by Cu-rich hydrothermal fluids, which chemically and thermally altered the first-stage bitumen, transforming it into pyrobitumen (R_0>0.7%). The following three sequential sub-stages, each one characterised by a special association of hydrothermal minerals and pyrobitumen types[1] are recognised (Table 1).

Main Cu-sulphide sub-stage The Cu-sulphide sequence starts with bornite I (with chalcopyrite I in ex-solution) and tetrahedrite I replacing pyrite (Fig. 4c). Bornite I + chacopyrite II in turn is replaced by chalcopyrite III along crystallographic planes (Fig. 4d). The Cu sulphides fill veinlets and contraction cracks (Fig. 4e) of isotropic, to weakly anisotropic, pyrobitumen (pyrobitumen I). This textural relationship indicates that bitumen was present in the host rock before the arrival of Cu-rich fluids. This mineral association occurs in zones of strong hydrothermal silicification (veins of quartz and colloform bands of chalcedony), pervasive chloritisation and zeolitisation.

Banded Cu-sulphide sub-stage This sub-stage, characterised by veinlets or irregular masses of bornite II + chalcopyrite II + tetrahedrite II (with colloform bands; see Fig. 4f,g) attached with calcite III (Fig. 5d) and quartz, appears only at the La Culebra mine. Chalcopyrite III fills

[1] The physical and optical characteristics of bitumen and pyrobitumen are explained in the next section ("Solid hydrocarbons: bitumen and pyrobitumen").

Table 1 Summary of characteristics for the Ocoita-Pabellon Metallotect (Copiapó Region)

	HYDROTHERMAL EVENTS			
	Fe-rich fluid	**Cu-rich fluid**		
	Bitumen and Fe-sulphide stage	**substage 1: Main Cu-sulphides**	**substage 2: Banded Cu-sulphides**	**substage 3: Enriched Cu-sulphides**
Bitumen R_0: measured reflectance of bitumen R_v: calculated reflectance of vitrinite $R_v = (R_0+0.414)/1.09$[a] $T_{peak} = (\ln Rv+1.19)/0.00782$[b]	**Bitumen** Isotropic R_0 (mean)= 0.53% R_v= 0.87% T_{peak}= 134 ºC	**Pyrobitumen I** Slightly anisotropic R_0 (mean) = 0.85% R_v= 1.16% T_{peak}= 171ºC	**Pyrobitumen II** Anisotropic with mesophase structure R_0 (mean) = 5.95% R_v= 5.84% T_{peak}= 378ºC	**Pyrobitumen III** Moderate anisotropic R_0 (mean) = 3.32 % R_v= 3.43% T_{peax}: 310ºC
Sulphide Paragenesis	Pyrite cogenetic with bitumen	Cu sulphides replacing pyrite and filling contraction cracks or degasification pores in bitumen Paragenesis: Bornite I - Chalcopyrite I Chalcopyrite II Tetrahedrite I	Coloform bands of: Bornite II Chalcopyrite III Tetrahedrite II	Replacement of bornite for: Chalcocite Covellite-digenite
S isotope in sulphides	δ^{34} S (py)= 0.6‰	δ^{34} S = -33.0 to -25.4 ‰	δ^{34} S = -44.7 to -31.7 ‰	δ^{34}S = -21.9 to -17.9 ‰
Calcite Paragenesis	Calcite I	Calcite II	Calcite III	Calcite IV
Fluid characteristics (from fluid inclusion study in calcite)	Median Th = 202 ºC S = 19 - 23 wt % NaCl eq. Te = -66.4 to -50.2 ºC Fluid system: H_2O-NaCl-$CaCl_2$	Median Th = 208 ºC S = 1 - 22 wt % NaCl eq. Te = -65 to -28 Fluid system: H_2O-NaCl-$CaCl_2$	Median Th = 246 ºC S = 6.6 - 23 wt % NaCl eq.	Median Th =175ºC S=17 - 25 wt % NaCl eq.
C and O isotope	Bitumen δC^{13} = -24.9 ‰	Bitumen δC^{13} = -25.2‰	Bitumen δC^{13} = -25.0‰ $\delta C^{13}_{calcIII}$ = -8.3 to -7.4‰ $\delta^{18}O_{calcIII}$= -11.0 to -10.3 ‰ $\delta^{18}O_{water}$= -7.8‰ (at 246°)	Bitumen δC^{13} = -25.0‰ δC^{13}_{calcIV}= -2.3‰ $\delta^{18}O_{calcIV}$= -17.5 ‰ $\delta^{18}O_{water}$= -14.6‰ (at 175°C)

[a]Landis and Castaño (1995)
[b]Barker and Pawlewicz (1994)

also the degassing porous of pyrobitumen (Fig. 4h) that, in this case, shows partial graphitisation, with mesophase microstructures (pyrobitumen II; Fig. 5c).

Enriched Cu-sulphide sub-stage This association involves the replacement of bornite II by chalcocite + digenite (Fig. 4i), in some cases generating complex myrmekitic textures (Fig. 4j) and finally by covellite + digenite (Fig. 4k). The associated gangue is chlorite, calcite and quartz. Small globules of hydrocarbon (pyrobitumen III) are co-genetic with chalcocite (Fig. 5d), suggesting that a new generation of liquid hydrocarbon could have been transported by the latest Cu-rich hydrothermal fluids.

Solid hydrocarbons: bitumen and pyrobitumen

The solid hydrocarbons, intimately associated with Cu and Fe sulphides, hydrothermal calcite, chlorite and quartz, fill the primary (vesicles) and secondary porosity (fractures) of the lavas, forming an interconnected network (Fig. 6a–c) or, locally, massive bands of Cu sulphides (Fig. 6d). In hand samples, the solid hydrocarbons appear as dark brown to black angular fragments, irregular masses or spherical globules (0.15 to 40 mm). These hydrocarbons are glassy with conchoidal fractures. Shrinkage cracks (resulting from the loss of volatiles and volume reduction during the solidification process) and degassing porosities (caused by heating and decompression) are commonly filled with ore and gangue minerals (Fig. 4e,h).

The solid hydrocarbons present at the lavas are allocthonous (from migrated source rocks), and consequently, according Jacob (1989) and Hunt (1978), they must be classified as “migrabitumen”. The micro-textures in the studied host rocks indicate that the hydrocarbons were fluids and viscous at the trapping time.

Based on GC analysis, Cisternas and Frutos (1996) interpreted the bitumen to have a general composition of 55.0% alkanes, 22.4% aromatic compounds, 21.9% NSOs and 0.7% asphaltenes, including a suite of “n-alkanes” between C^{12} and C^{36}, with a peak at C^{19} (GC–mass spectrometry) of the alkane fraction. As suggested by Cisternas et al. (1999a), the possible source for the solid hydrocarbons in the Copiapó area could be the organic matter contained in the underlying marine bituminous algal-mat facies of the upper part of the Nantoco Formation

(Cisternas and Diaz 1990). Studies to confirm this hypothesis are still in process.

Physical and optical properties

Solid hydrocarbons from the studied deposits are not soluble in CS_2, immersion oil or ether, and do not present fluorescence. Microscopically, under reflected light and using immersion oil, these hydrocarbons show a light-brown colour, being isotropic or moderately to strongly anisotropic (Fig. 7a–d). In some samples, these hydrocarbons display partially graphitised domains (mesophase microstructure, Figs. 5c and 7c), suggesting a thermal and/or chemical process that altered the previously formed pyrobitumen.

Following Landis and Castaño (1995), we used the random reflectance value and the anisotropy property to differentiate the two types of solid hydrocarbons. The term "bitumen" is used for isotropic or weakly anisotropic solid hydrocarbon with R_0<0.7%, and "pyrobitumen" for solid hydrocarbons with R_0>0.70% and **a** moderate-to-strong anisotropy (Fig. 7). At the studied deposits, the extractable organic-solvent fraction is notably more abundant in bitumen than in pyrobitumen (paper in process).

The statistical analysis of the random reflectance (R_0) results for 34 samples from the studied deposits (Fig. 7) indicates that the R_0 values (R_{0mean}) can be used to discriminate between bitumen and three types of pyrobitumen.

Bitumen (R_{0mean}=0.53%) is present only in samples from the San Pedro mine in the northern part of the district, where it appears associated with pyrite, chlorite and calcite I (Figs. 4a,b; 6c; and 7a). Pyrobitumen I (R_{0mean}=0.85%), associated with bornite I–chalcopyrite I, chalcopyrite II–tetrahedrite I and calcite II, is present in samples from the Manto Cobriza and the La Culebra mines (Fig. 7b). Pyrobitumen II (R_{0mean}=5.84%) occurs with banded bornite II–chalcopyrite III–tetrahedrite II and calcite III only in some samples from the La Culebra mine (Figs. 5c and 7c). Pyrobitumen III (R_{0mean}=3.43%) appears with chalcocite and covellite–digenite in samples from the Gloria-Chinches mine, in the southern part of the district (Figs. 5d and 7d).

If R_{0min} is plotted against R_{0max}, the samples clearly group in four populations (Fig. 8), with the isotropic and weakly anisotropic samples close to the line R_{0max}=R_{0min}, the moderately anisotropic samples to the left and the strong anisotropic samples to the upper left. According to Goodarzi et al. (1993), this graph can be used to reconstruct the thermal evolution of the solid hydrocarbons. Therefore, assuming the same type of "starting" material, the bitumen represents the hydrocarbons mobilised by the Fe-rich hydrothermal fluids, whereas the three pyrobitumen groups represent, as a whole, the alteration products of the Cu-rich hydrothermal event. In more detail, bitumen (isotropic) represents the Fe-sulphides stage, pyrobitumen I (isotropic to weakly anisotropic) the *Main Cu-sulphides sub-stage*, pyrobitumen II (strongly anisotropic, partially graphitised with mesophase microstructure) represents the *Banded Cu-sulphides sub-stage*, and pyrobitumen III (moderate anisotropic) represents the *Enriched Cu-sulphides sub-stage* (Fig. 8).

Reflectance as a geothermometer

To use the reflectance data as a geothermometer (Fig. 7), it is first necessary to calculate the equivalent vitrinite reflectance values (R_v) according to the method of Landis and Castaño (1995), which uses the expression $R_v = (R_0 bit + 0.414)/1.09$. Using R_v as the empirical Barker and Pawlewicz (1994) geothermometer, the maximal hydrothermal temperature (T_{peak}) was calculated as follows: $T_{peak} = (\ln(R_v) + 1.19)/0.00782$.

Considering the paragenetic position of the types of solid hydrocarbons (Fig. 7; Table 1), the calculated T_{peak} can be applied to detect the thermal overprint of the successive mineralisation stages on a background thermal level. In this way, the temperature of 134°C obtained from the bitumen reflectance indicates the temperature of the Fe-rich hydrothermal fluids and, indirectly, the possible maximal regional maturation level, while the T_{peak} values calculated from the reflectance data of pyrobitumen record the temperatures of the Cu-rich hydrothermal fluids, which physically and chemically altered the original bitumen. The formation of pyrobitumen I (thermal degassing and volume loss by contraction of previously less mature bitumen) occurs at a temperature of about 170°C, associated with the circulation of the first hydrothermal Cu-rich fluids. A rise in the mineralisation temperature to a peak of about 380°C is registered by the partially graphitised pyrobitumen II associated with banded Cu sulphides present exclusively at the La Culebra mine. A decrease to about 310°C during the last hydrothermal sub-stage is registered by the moderate anisotropic pyrobitumen III present as small globules in the latter Cu sulphides. Later, we will compare these values with the thermometric data obtained from the fluid inclusions study of hydrothermal calcite.

Fluid inclusions and hydrothermal fluids characteristics

Representative samples of the four paragenetic stages (Table 1) were selected to study the fluid inclusions of the hydrothermal calcite. This study demonstrated three populations: (a) the most common primary fluid inclusions consist of a population of two-phase (L+V, liquid-rich) inclusions that occur in isolated form or along crystallographic planes of the host calcite; (b) the second group consists of three-phase inclusions, containing crude oil, and (c) the third population consists of two-phase (L+V, vapour-rich) inclusions. Thermometric data were collected only from the first group (two-phase, liquid-rich inclusions), for which the size ranged between 5 and 30 μm. Fluid salinities (expressed as weight percent NaCl eq.) were calculated using the method of Potter et al. (1978).

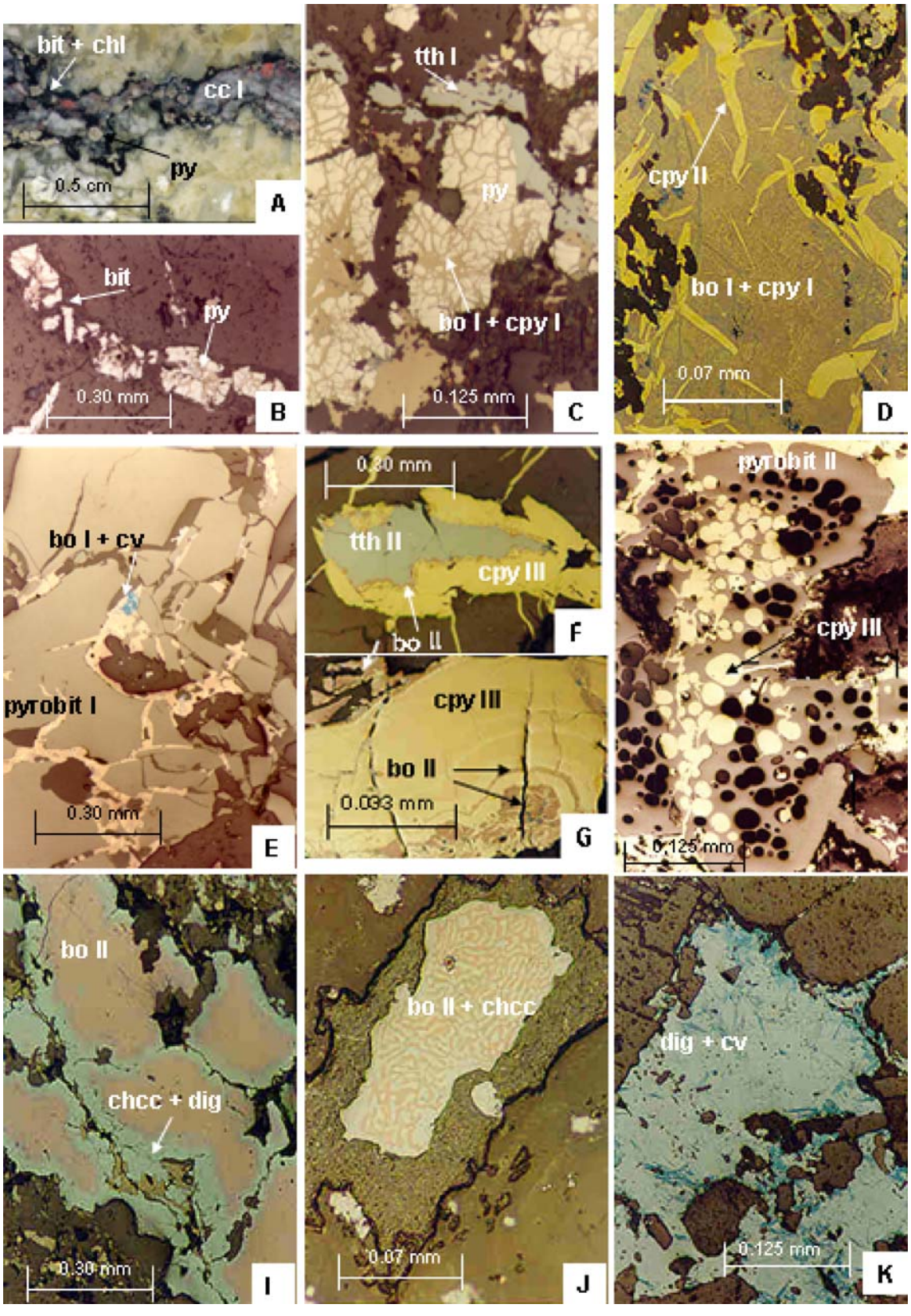

Because each calcite generation is related to a hydrocarbon thermal alteration stage, the objective of this fluid inclusion study was to compare the thermometric data from fluid inclusions with the thermometric data from vitrinite equivalent reflectance. Consequently, in the samples used for the fluid inclusion study, the reflectance of solid

◀ **Fig. 4** Paragenetic sequence for Fe and Cu sulphides. *Fe-rich hydrothermal event*: **a** Close-up of sequential textures of bitumen, chlorite, pyrite and calcite in a veinlet. **b** Microphotograph (reflected light) of a veinlet filled with bitumen–chlorite on the edges and pyrite in the centre. *Cu-rich hydrothermal event*: **c** Reflected light microphotograph showing bornite I + chalcopyrite II and tetrahedrita I replacing pyrite. **d** Detail view of **c** showing the exsolution texture between bornita I and chalcopyrite I, in turn replaced by chalcopyrite II (reflected light). **e** Reflected light microphotograph showing bornite I filling contraction cracks of pyrobitumen I. **f** Reflected light microphotograph of veinlet of chalcopyrite III bornite II and tetrahedrite II associated with pyrobitumen II. **g** Detail view of **f**, showing the colloform bands of chalcopyrite III and bornite II. **h** Reflected light microphotograph of chalcopyrite III infilling the degassing pores of pyrobitumen II. **i** Reflected light microphotograph showing the replacement of bornite II by chalcocite + digenita. **j** Reflected light microphotograph highlighting myrmekitic textures between bornite II and chalcocite. **k** Reflected light microphotograph displaying the total replacement of bornite II by covellite + digenite. Abbreviations: *bit*, bitumen; *bo*, bornite; *cc*, calcite; *chcc*, chalcocite; *chl*, chlorite; *cpy*, chalcopyrite; *cv*, covellite; *dig*, digenite; *py*, pyrite; *pyrobit*, pyrobitumen; *tth*, tetrahedrite. *Roman numbers* represent the paragenetic stages

hydrocarbons was also measured. Figure 9 presents the measured homogenisation temperatures plotted against the reflectance data of solid hydrocarbons, while Fig. 10 presents the range and median of the calculated saline compositions for each generation of calcite

In the *Fe sulphides stage*, the vesicles of the lavas, and the veinlets interconnecting them, were filled with calcite I together with quartz, chlorite, bitumen ($R_0 \leq 0.7\%$) and pyrite (Fig. 5a). The inclusions measured in calcite I have V_L/V_T ratios between 0.80 and 0.97, and sizes between 10 and 30 μm.

The homogenisation temperatures for calcite I in the Fe-sulphides-stage samples range between 134 and 307°C. The temperatures below 150°C probably represent the temperature of the fluid that mobilised the hydrocarbons towards the host rock, because these values are coincident with the thermometric data measured in oil inclusions (Th_{oil}, in the range 115–140°C, as reported by Cisternas et al. 1999b). Values over 200°C are coincident with geothermometric data from Fe-rich chlorites (co-genetic with bitumen), indicating temperatures between 190 and 299°C (Cisternas et al. 1999a). The calculated saline compositions are very homogenous, ranging between 19 and 23 wt.% NaCl eq. (Fig. 10).

In the *Main Cu-sulphides sub-stage*, the veinlets that cut the vesicles of the previous phase were filled with calcite II (Fig. 5b) together with pyrobitumen I (R_0=0.9%), chalcopyrite I and II, bornite I and tetrahedrite I. The fluid inclusions hosted in calcite II have V_L/V_T ratios between 0.80 and 0.97, and are more difficult to observe due to their smaller size. The results indicate homogenisation temperatures (*Th*) between 116 and 291°C, with a median of 208°C (Fig. 9), similar to those of the Fe-rich sulphide stage (calcite I). The salinities range between 3.5 and 22.4 wt.% NaCl eq., with the majority concentrated around 20 wt.% NaCl eq. (mode at 20.9 wt.% NaCl eq., Fig. 10).

Calcite III (Fig. 5c), present in the *Banded Cu-sulphide stage*, is related to pyrobitumen II (graphitised pyrobitumen of strong anisotropy and R_0=5.72%) and appears in banded veinlets next to bornite II, chalcopyrite III and tetrahedrite II (Fig. 5d). Fluid inclusions hosted in calcite III have V_L/V_T ratios between 0.50 and 0.97. The homogenisation temperatures (*Th*) range from 120 to 404°C, with a median value of 246°C, which is the highest median value of all calcite generations (Fig. 9). The fluid inclusions in calcite III present a wide salinity range, between 6.6 and 24 wt.% NaCl eq., with a median at 20 wt.% NaCl eq. (Fig. 10).

In the *Enriched Cu-sulphides sub-stage*, which represents the last mineralisation phase, calcite IV (containing globules of pyrobitumen III with R_0=3.83%) is related to chalcocite, covellite and digenite (Fig. 5d). The homogenisation temperatures range from 130 to 353°C, with a median of 209°C (Fig. 9). The salinities range between 17.0 and 25.3 wt.% NaCl eq., with a median value of 19.8 wt.% NaCl eq. (Fig. 10).

The plotting of the homogenisation temperatures (*Th*) against the reflectance values of the solid hydrocarbon of

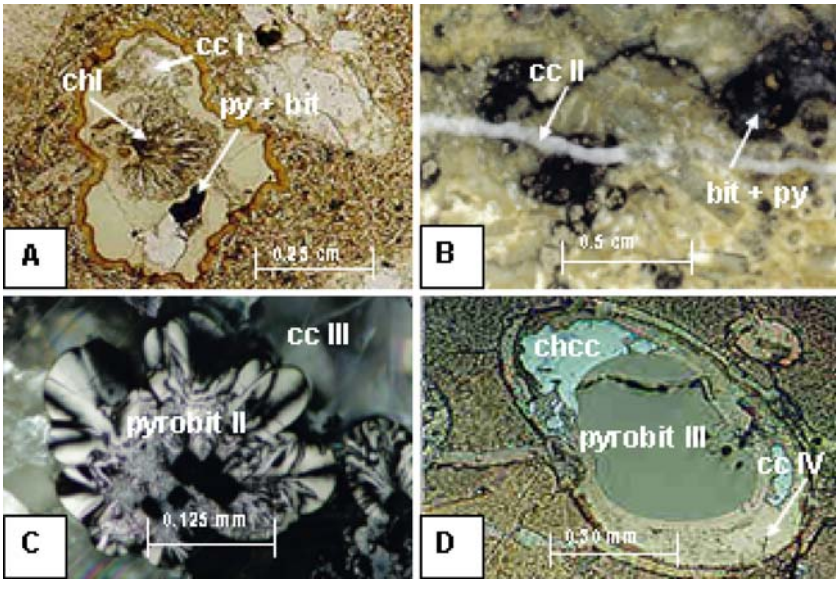

Fig. 5 Hydrothermal generations of calcite. **a** Microphotograph of primary vesicles of the porphyritic lavas filled with calcite I, associated with bitumen, pyrite and chlorite (transmitted plane polarised light). **b** Close-up photo of a veinlet of calcite II cutting the primary vesicles of the lavas. **c** Reflected light microphotograph showing calcite III associated with graphitised pyrobitumen II. **d** Reflected light microphotograph of a globule filled with calcite IV, pirobitumen III and chalcocite. For abbreviations, see Fig. 4

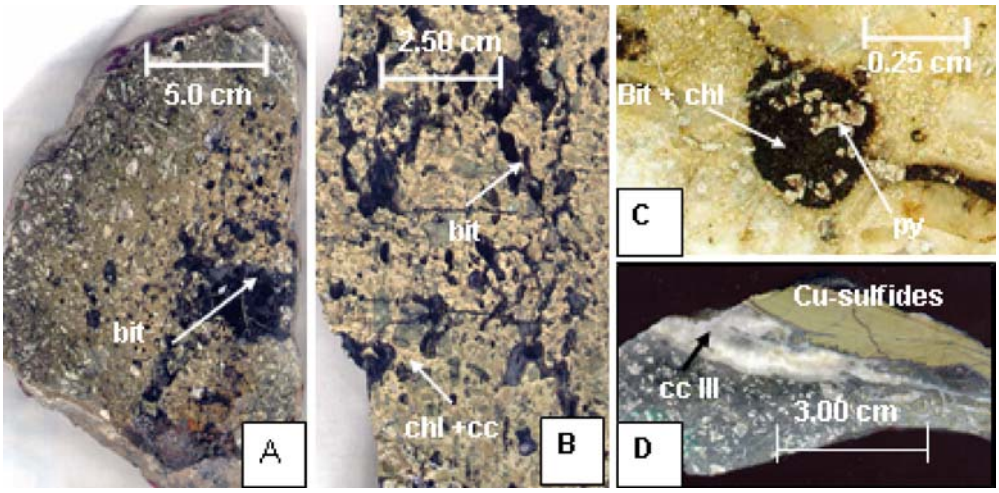

Fig. 6 Hand specimen photographs of porphyritic lavas host rocks. **a** and **b** primary (vesicles) and secondary porosity (veinlets) of the lavas filled with solid hydrocarbons, chlorite and calcite. Note the interconnected network. **c** Detail view of a vesicle filled with bitumen (*bit*), chlorite (*chl*) and pyrite (*py*). **d** Banded Cu sulphides typical of the La Culebra mine. For abbreviations, see Fig. 4

the same sub-stage (Fig. 9) shows a broad dispersion for all calcite generations, indicating that more than one calcite generation probably coexists in the samples. Nevertheless, the *Th* median of each population is similar (around 200°C), with the exception of the calcite III, whose median is obviously higher (246°C). Coincidentally, calcite III is associated with pyrobitumen II, which has the highest reflectance values, strong anisotropic domain and mesophase microstructure between pyrobitumen and graphite (Fig. 5c).

For comparison, the temperatures calculated from the thermal maturity of hydrocarbons are indicated in Fig. 9 (T_{peak} was calculated according to the method of Barker and Pawlewicz, explained in Fig. 7). In the initial stages (corresponding to calcite I and II) expressed in a lower degree of thermal maturity (R_0<1.0%), the calculated T_{peak} is less than the *Th* medians. This tendency is reversed in the stages of greater thermal alteration (calcite III and IV), where the T_{peak} is significantly higher than the *Th* medians.

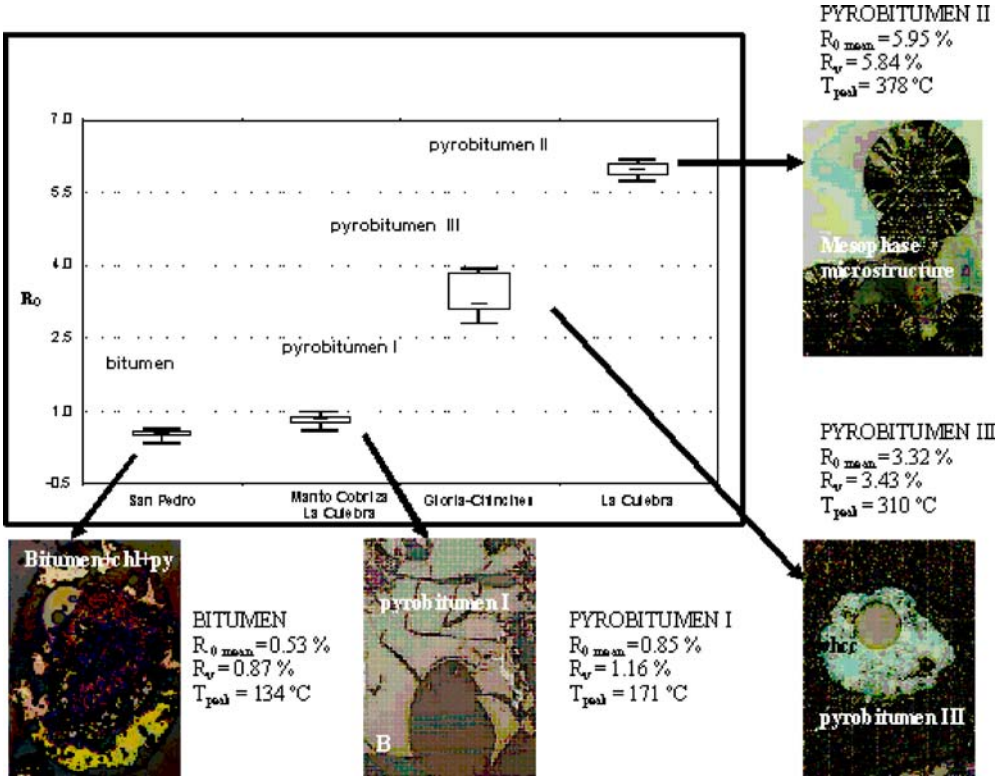

Fig. 7 Ranges and medians of random reflectance of solid hydrocarbons (R_0) from deposits of Ocoita-Pabellon Metallotect. To calculate R_v, we use the mean value of R_0 (R_{0mean}). $R_v = (R_0 + 0.414)/1.09$, according Landis and Castaño (1995). $T_{peak} = (\ln R_v + 1.19)/0.00782$, according Barker and Pawlewicz (1994). Abbreviations: *py*, pyrite; *cpy*, chalcopyrite; *chcc*, chalcocite; *chl*, chlorite. *Roman numbers* represent the paragenetic stages

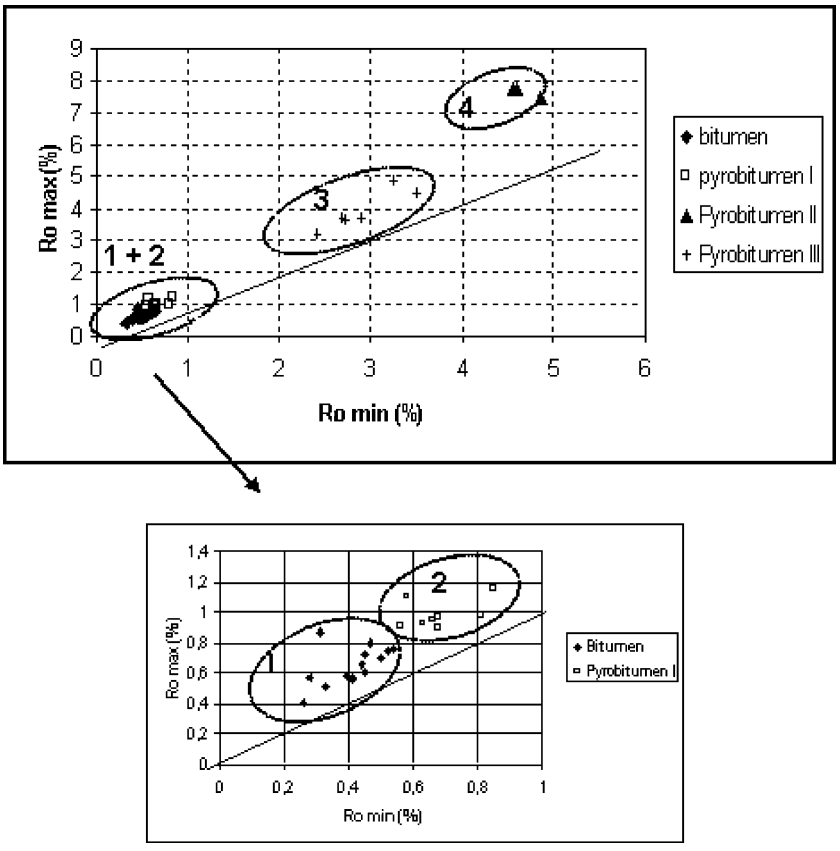

Fig. 8 Plot of R_{0min} against R_{0max} of bitumen and pyrobitumen. The *line* represent R_{0min}= R_{0max}. *Group 1* correlates with the Fe-rich hydrothermal event. *Groups 2*, *3* and *4* correlate with the Cu-rich hydrothermal event. See text for discussion

Using two independent methods as geothermometers (fluid inclusion thermometry and solid hydrocarbon reflectance), we can conclude that the temperature of the Fe-rich hydrothermal event was similar to the first stage of the Cu-rich event. The evolution of the hydrothermal system then continued to higher temperatures in the following sub-stages of the Cu-rich event. Locally, in the area of the La Culebra mine, greater temperatures are recorded (up to 400°C), altering the pyrobitumen more

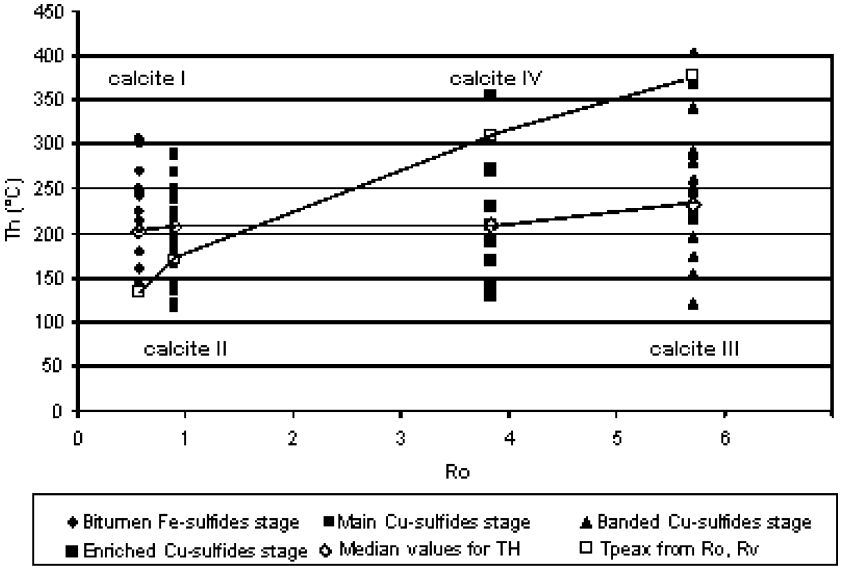

Fig. 9 Range and medians of the homogenisation temperature (*Th*) of fluid inclusions in hydrothermal calcites against R_0 (from bitumen and pyrobitumens). The T_{peak} was plotted for comparison (see Fig. 7)

Th°C	N	Mean	Median	Mode	Min	Max	SD
calcite I	17	194	202	142	134	307	59.86
calcite II	30	195	208	135	116	291	58.65
calcite III	23	251	246	221	120	404	73.98
calcite IV	9	208	209		130	353	20.70

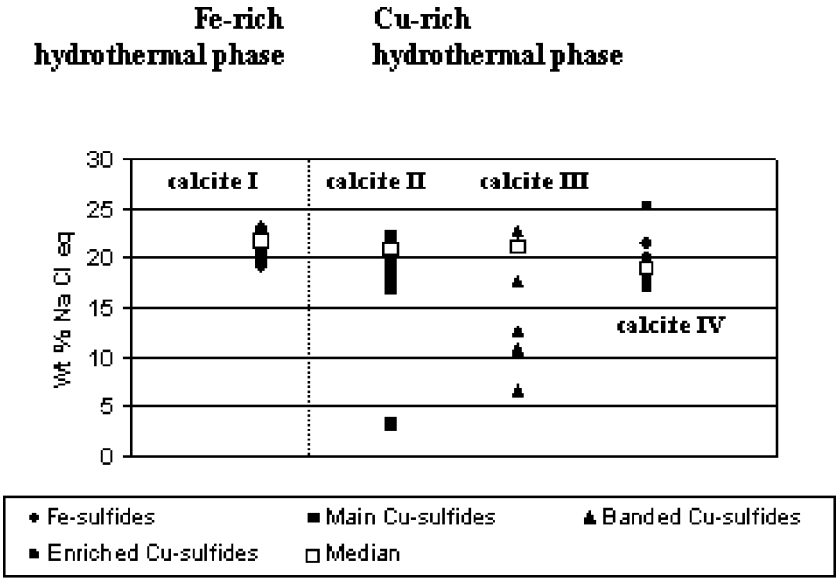

Fig. 10 Range and medians of the salinities of fluid inclusions in hydrothermal calcites

Th°C	N	Mean	Median	Min	Max	SD
calcite I	17	21.3	21.8	19.1	23.2	1.30
calcite II	28	16.3	20.9	3.5	22.4	5.66
calcite III	7	14.9	21.4	6.6	22.7	6.19
calcite IV	6	19.8	19.2	17.0	25.3	3.07

intensely (pyrobitumen II, R_0>6.0%, with partially graphitised domains).

The salinity data dispersion patterns are similar for the calcite I, II and IV, but calcite III presents a greater dispersion (Fig. 10). Nevertheless, if we consider the

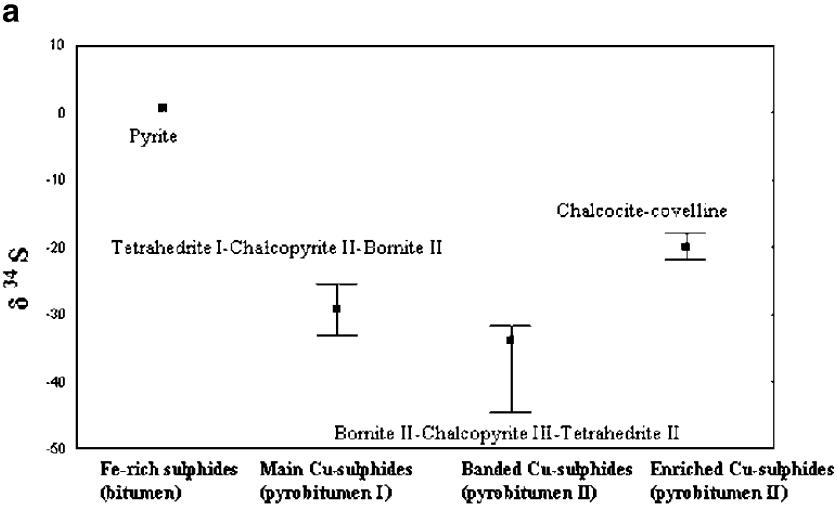

Fig. 11 Ranges and medians of $\delta^{34}S$ in sulphides from the different hydrothermal sub-stages

b

	Fe-rich hydrothermal phase	Cu-rich hydrothermal phase		
	Fe-sulfides Pyrite	Main Cu-sulfides Tetrahedrite I Chalcopyrite I Bornite I	Banded Cu-sulfides Tetrahedrite II Bornite II Chalcopyrite III	Enriched Cu-sulfides Chalcocite Covellite
N	1	2	4	2
Mean		-29.0	-35.7	-19.8
Median	0.6	-29.2	-34.0	-19.9
Min		-25.4	-31.7	-17.9
Max		-33.0	-35.7	-21.9
SD		5.37	6.02	2.83

medians (between 19.2 and 21.8 wt.% NaCl eq.), the four calcite generations show a similar tendency, indicating a near constant pore-fluid salinity across the region and across time. The scarce data below 10 wt.% NaCl eq. (from calcite II and III) could be related to a partition process of the hydrothermal fluid as a consequence of fluid boiling or mixture. However, no direct evidence was found that could confirm the boiling process, except for the coexistence of inclusions rich in liquid and inclusions rich in vapour in calcite III. The saline compositions are congruent with the fluid compositions deduced from the temperatures of the eutectic points (T_e between −66 and −28°C), only registered in inclusions from calcite I and II, suggesting complex fluids, probably with the participation of $CaCl_2$ and $MgCl_2$ in addition to NaCl (Davis et al. 1990).

S, C and O-isotopes

Sulphur isotope analyses were carried out on sulphide concentrates representative of the hydrothermal stages, as shown in Fig. 11. The $\delta^{34}S$ values of pyrite and subsequent Cu sulphides are different, with a broad range of variation between Fe and Cu sulphides (from 0.6 to −44.7‰ V-CDT). Pyrite, representing the Fe-rich hydrothermal phase, presents notably heavier $\delta^{34}S$ values (mean=0.6‰ V-CDT) than found overall for the Cu sulphides of the Cu-rich hydrothermal phase (mean=−28.2‰ V-CDT). For the three individual sub-stages of the Cu-rich hydrothermal phase (Fig. 11), all $\delta^{34}S$ values are notably negative, with $\delta^{34}S$ ratios ranging between −33.0 and −25.4‰ V-CDT in sulphides for the *Main Cu-sulphides sub-stage* (tetrahedrite I and chalcopyrite II–bornite I); between −44.7 and −31.7‰ V-CDT for the *Banded Cu-sulphides sub-stage* (bornite II–chalcopyrite III and tetrahedrite II), and between −17.9 and−21.9‰ V-CDT for the last *Enriched Cu-sulphides sub-stage* (bornite II–chalcocite–covellite).

The interpretation of sulphur isotope ratios for sulphides associated with hydrothermal systems is difficult unless the host rocks' isotopic compositions and local Redox relationships are known (Ohmoto 1972). In the studied samples, the sulphides with the lightest $\delta^{34}S$ values (averaging near −35‰) are related to the *Banded Cu-sulphides sub-stage* with strongly chemically and physically altered pyrobitumen II (anisotropic, partially graphitised with mesophase microstructure and R_0>6%).

Notwithstanding, negative $\delta^{34}S$ values are normally related to biogenic sulphide formed by bacterial reduction of marine sulphate at T<100°C, but these values could also be explained as isotopic fractionation between in-equilibrium sulphide species, where the pH and f_o play an important role. Thus, if pH diminishes and the f_o increases in the mineralising environment, magmatic sulphur could be fractionated and the subsequent sulphides could have very light $\delta^{34}S$ values, similar to those formed in the presence of biogenic sulphur.

Considering the distinctly different $\delta^{34}S$ values between the pyrite and the Cu sulphides that replaced them, the $\delta^{34}S$ values suggest overall that the source of S for the Fe-rich phase could be different from the source of S for the Cu-rich hydrothermal phase. The source of S to form pyrite, being near zero ($\delta^{34}S$=0.6‰), could be magmatic,

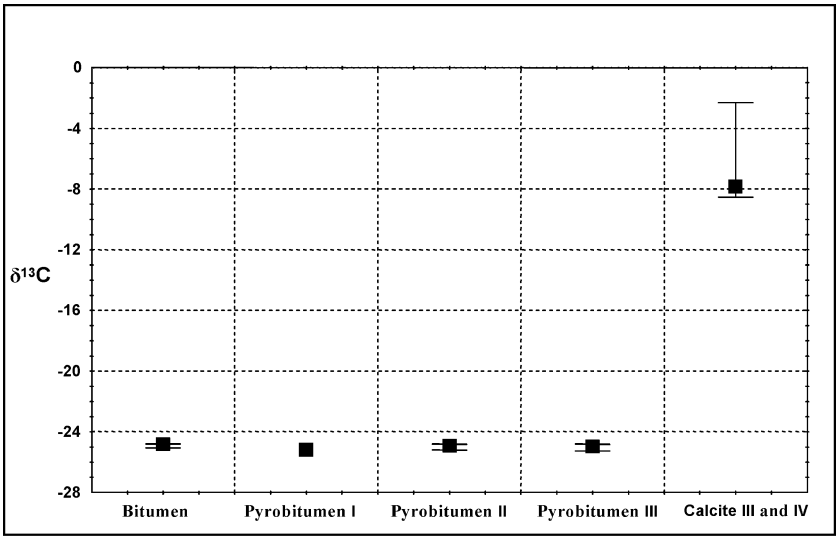

Fig. 12 Ranges and medians of $\delta^{13}C$ in bitumen, pyrobitumens (I, II and III) and late calcites (III and IV)

	Bitumen	Pyrobitumen I	Pyrobitumen II	Pyrobitumen III
N	3	1	3	3
Mean	24.9	25.2	25.0	25.0
Median	24.8		24.9	25.0
Min	24.8		24.8	24.8
Max	25.1		25.2	25.3
SD	0.14		0.20	0.23

whereas the source for the Cu sulphides is uncertain but highly improbable to have been inherited from pyrite.

A biogenic origin of the S is not probable either because the temperatures of the hydrothermal Cu-rich event are too high (150 to 400°C) to allow the existence of reducing sulphate bacteria. If there had been bacteria participation, then it must have taken place in low-temperature zones (<100°C) and the H_2S produced there would have been collected by the hydrothermal fluids that finally arrived in the host rock where the sulphides formed.

The $\delta^{13}C$ of the bitumen and pyrobitumen, with an average value of −25‰ (whole extract), is similar in all stages of pyrobitumen (Fig. 12) and in the organic fractions (alkanes, $\delta^{13}C$=−25.6‰; aromatic, $\delta^{13}C$=−23.5‰; Cisternas et al. 1999a), indicating that the bitumen and pyrobitumen were derived from hydrocarbons. Our results are comparable to the $\delta^{13}C$ of bitumen at the El Soldado deposits, where the $\delta^{13}C$ ranges from −26 to −30‰ V-PDB (Wilson 1998; Wilson et al. 2003b).

The $\delta^{13}C$ isotopic compositions of calcite could only be determined for calcite III and IV. The values range from −2.3 to −8.3‰ V-PDB (Figs. 12 and 13), suggesting some involvement of C derived by thermal degradation of bitumen or incorporation of carbonate-bearing meteoric waters. Similar to sulphur, the isotopic composition of carbon in hydrothermal carbonates depends on numerous variables: the C source, the oxygen fugacity, the pH, the temperature and the total carbon concentration (Ohmoto 1972; Rye and Ohmoto 1974). Where organic matter is present, the maturity is also a factor because a greater thermal maturation results in ^{13}C enrichment (Lewan 1983). Late-stage carbonates generally present enrichment in the heavy isotope relative to the early phase as a result of ore-fluid cooling, decreasing CO_2/CH_4 ratios in the fluid, and/or an increasing contribution of CO_2 from others sources (Hoefs 1987). The range of our $\delta^{13}C$ results (coincident with various hydrothermal ore deposits; see Hoefs 1987) could be generated by simple mixing between carbonate-derived and organically derived CO_2. The carbonate-derived CO_2 could come from the decarbonation of calcareous rocks during the hydrothermal influx and/or from carbonate-bearing meteoric waters. According to Longstaffe and Ayalon (1987), calcite formed under high pressure and temperature and in the presence of abundant meteoric water has $\delta^{13}C$ values around −7.1‰. Lighter organic carbon would be derived from pyrobitumen maturation.

The plot of $\delta^{13}C$ vs $\delta^{18}O$ ratios (Fig. 13) presents a different C–O signature for the hydrothermal calcites III and IV. Calcite IV, associated with the late *Enriched Cu-sulphides sub-stage*, displays heavier $\delta^{13}C$ (−2.3‰ V-CTD) and lighter $\delta^{18}O$ (−17.5‰ V-SMOW) values when compared to calcite III, associated with the *Banded Cu-sulphides sub-stage* ($\delta^{13}C$=−8.1‰ V-CTD; $\delta^{18}O$=−10.7‰ V-SMOW).

Fluid $\delta^{18}O$ values were calculated according to the fractionation factor of O'Neil et al. (1969), using the median homogenisation temperature (*Th* median) measured in the fluid inclusions of calcite III and IV (Table 1, Fig. 13). The hydrothermal fluids associated with the *Banded Cu-sulphides stage* (calcite III) have an $\delta^{18}O$ value of −7.8‰ V-SMOW at 246°C, whereas fluids associated with the *Enriched Cu-sulphides sub-stage* (calcite IV) yield a value of −14.6‰ V-SMOW at 175°C. These results, even with the limited number of samples analysed in this study, suggest the increasing participation of meteoric waters in the late stages of the hydrothermal system.

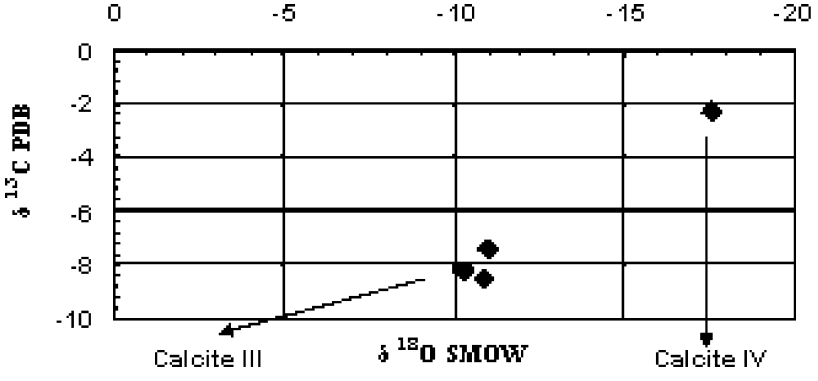

Fig. 13 $\delta^{13}C$ vs $\delta^{18}O$ in late hydrothermal calcites

Paragenesis substage	$\delta^{13}C$‰ PDB	$\delta^{18}O$‰ SMOW	calculel $\delta^{18}O_{fluid}$‰
Calcite III (Banded Cu-sulphides)	-7.4	-11.0	
	-8.5	-10.9	
	-8.3	-10.3	-7.8
Calcite IV (Enriched Cu-sulphides)	-2.3	-17.5	-14.6

Conclusions

The volcanic host rocks of the Ocoita-Pabellón Metallotect were extruded in a transitional shallow marine to sub-aerial environment, in an extensional tectonic setting during the late stage of the Cretaceous backarc basin. The main maturation mechanism of the rich organic matter underlying marine sedimentary units during burial was the increasing regional heating associated with the extension and thinning of the backarc basin floor. Additionally, Cretaceous magmatism contributed to the thermal maturation. Hydrocarbons were collected by Fe-rich hydrothermal fluids and introduced in the overlying host rocks using the primary and secondary porosity of the Pabellón Formation lava belt. The fluids-inclusion thermometry in hydrothermal calcites supports the reflectance results for solid hydrocarbons (bitumen and pyrobitumen), indicating a high degree of maturation attributed to prolonged hydrothermal alteration. The progressive thermal alteration of hydrocarbons during interaction with the hydrothermal fluids explains the formation of three generations of pyrobitumen.

The mineralogical, textural, fluid inclusion and isotope studies performed on the four mineral deposits of the Ocoita-Pabellón Metallotect (Table 1) indicate two distinct hydrothermal ore-forming events: (a) an early Fe-rich stage associated with the migration and emplacement of oil, and the formation of pyrite as the first sulphide, and (b) a late Cu-rich stage (with three consecutive sub-stages), where the pyrobitumen induced reduction and Cu-sulphide precipitation. The paragenetic sequence and the main characteristics for the two ore-forming events are summarised in Table 1.

Early Fe-rich hydrothermal event: bitumen–iron sulphides

During the earlier Fe-rich event, petroleum migrated as a discrete hydrocarbon phase accompanied by hydrothermal water at temperatures of 100–150°C. Temperatures increased when the first hydrothermal minerals (pyrite, calcite I, chlorite) precipitated (Bitumen *Fe-sulphides stage*) (median *Th*=202°C in calcite I). The bitumen of this phase (isotropic with low reflectance, R_0 between 0.4 and 0.7%) displays a moderate degree of maturation. The sulphur isotopic signature of pyrite ($\delta^{34}S$=0.6‰ V-CDT) indicates a magmatic sulphur source.

Subsequent Cu-rich hydrothermal event

Due to subsequent heating, bitumen began to degas and crack, forming pyrobitumen. The open spaces generated were filled first with calcite II and later with copper sulphides. Copper was probably transported as chloride complexes in oxidised fluids and precipitated Cu sulphides, when the fluids reacted with bitumen and pyrite from the previous phase.

During the first sub-stage of the Cu-rich hydrothermal event (*Main Cu-sulphides sub-stage*), temperatures were near 200°C (median *Th*=208°C in calcite II). Pyrite was replaced by chalcopyrite I and II + bornite I + tetrahedrite I. Those minerals, together with calcite II, precipitated in contraction cracks and gas vesicles of the pyrobitumen I. The pyrobitumen I is slightly anisotropic and has a reflectance close to 1%. The $\delta^{34}S$ values of the early Cu sulphides (from −25.4 to −33.0‰ V-CDT) indicate that sulphur probably was not inherited from pyrite alone during its replacement by Cu sulphides.

During the second Cu-rich sub-stage, found only at the La Culebra mine, calcite III + chalcopyrite III + bornite II + tetrahedrite II precipitated in banded veins (*Banded Cu-sulphides sub-stage*). The higher temperature of this phase (median *Th*=246°C in calcite III) produced a strong thermal alteration of pyrobitumen I, expressed by a higher reflectance (R_0>6%), anisotropy and mesophase structure between pyrobitumen and graphite (pyrobitumen II). The sulphur isotope signature of the sulphides from this phase is markedly negative ($\delta^{34}S$=−31.7 to −44.7‰ V-CDT).

In the late Cu-rich sub-stage, the temperature decreased (median *Th*=208°C in calcite IV) and chalcocite, covellite and digenite precipitated (*Enriched Cu-sulphides sub-stage*). In this sub-stage, small globules of pyrobitumen III (R_{0mean}=3.32%) appear in the sulphides. The $\delta^{34}S$ of these latest sulphides are slightly heavier than in the previous sub-stages (mean $\delta^{34}S$=−18.8‰ V-CDT).

The $\delta^{13}C$ of calcite and the calculated $\delta^{18}O$ values of water (−7.8 to −14.6‰) in equilibrium with calcite (calcite III and IV) in the last two sub-stages of the Cu-rich event suggest the participation of meteoric waters in the hydrothermal system. This explanation is in agreement with the structural position of the host rocks (the mineralisation occurs before the tectonic inversion of the basin) and the shallow depths at the Upper Cretaceous plutons (1,700- to 2,000-m depth, Marschik and Fontboté 2001) were intruded. However, the salinities in hydrothermal calcite from the Cu-rich sub-stages (median value around 20 wt.% NaCl eq.) require that the meteoric fluid mix with a second fluid of considerably higher salinity.

Comparison with the other deposits and exploration potential

The results presented in this paper demonstrate the strong genetic and temporal relationship between copper and pyrobitumen in the deposits of the Ocoita-Pabellón Metallotect in the Copiapó Region and stress the importance of pyrobitumen as a prospecting tool in a regional context. The same close relationship between pyrobitumen and copper sulphides has been established for other Cu-mineral deposits hosted in Lower Cretaceous sequences in central Chile; for example, the El Soldado (Wilson 1998, 2000; Boric et al. 2002; Wilson et al. 2003a,b), a large manto-type deposit, where pyrobitumen is intimately associated with Cu sulphides.

As was pointed out by Haggan et al. (2003), a comparison between the deposits of the Copiapó Region (Ocoita-Pabellón Metallotect) and the El Soldado ore deposit indicates notable similarities, such as the same age for the host rocks, similar types of hydrothermal stages, an early Fe-rich stage associated with oil migration and emplacement and a late, Cu-rich phase where the bitumen induced reduction and sulphide precipitation.

Thus, the present work confirms similarities to mineralisation studies by previous workers, while emphasising some important differences, such as:

1. Pyrite origin: At El Soldado, the pyrite is framboidal, implying formation assisted by bacteria (Wilson et al. 2003a). In the Ocoita-Pabellón Metallotect, pyrite is clearly hydrothermal without any indications of diagenetic origin.
2. Sulphur origin: At El Soldado, the $\delta^{34}S$ values for pyrite (between −11.1 and 28.0‰) are similar to the subsequent Cu sulphides ($\delta^{34}S$ between −12.7 and 19‰), indicating that sulphur was inherited from the pyrite during its replacement (Wilson 1998; Wilson et al. 2003b). In contrast, at the Ocoita-Pabellón Metallotect, the $\delta^{34}S$ values of pyrite and copper sulphides are different (a difference of about −45‰), with a distinctive light $\delta^{34}S$ signature for Cu sulphides ($\delta^{34}S$ between −44.7 and −17.9) suggesting different sources or strong isotope fractionation. Notably, the $\delta^{34}S$ values of the Cu sulphides from the deposits of Copiapó are comparable to the $\delta^{34}S$ values of diagenetic Cu sulphides from the organic matter-rich Veta Negra deposit, located stratigraphically above the El Soldado deposit in central Chile.
3. Carbon isotope signature of pyrobitumen: The $\delta^{13}C$ values of pyrobitumen between El Soldado and the deposits of Copiapó are comparable, although the range is wider for El Soldado (−26 to −30‰ V-PDB, Wilson 1998; Wilson et al. 2003b), whereas in the Ocoita-Pabellón Metallotect, the values are markedly constant (−24.9 to −25.2‰ V-PDB, without evidence of fractionation related to the maturation).
4. Migration mechanism of hydrocarbons: The paragenetic and spatial relationships of bitumen with hydrothermal species such as pyrite, chlorite and calcite indicate that the bitumen was collected from the source rocks or from a hydrocarbon reservoir for Fe-rich hydrothermal fluids.
5. Sources for the mineralising fluids: Whereas the oxygen isotope ratios of water in equilibrium with calcite for the El Soldado are concordant with a basin connate-metamorphic brine origin ($\delta^{18}O$=6.4 to 11.5‰; Boric et al. 2002; Wilson et al. 2003b), the values for the studied deposits of Copiapó (Ocoita-Pabellón Metallotect) are distinctively lower ($\delta^{18}O$= −7.8 to −14.6‰ for the Cu-rich stage), indicating the participation of meteoric water in the hydrothermal system.

The genetic model, presented in this work for the Copiapó Region (Ocoita-Pabellón Metallotect), relates the Cu(Fe)-mineralisation processes with the presence of solid hydrocarbons in the primary and secondary porosity of the porphyritic lavas ("ocoitas"). This model can be used as an exploration tool for similar deposits in the more than 500-km-long stretch of the Lower Cretaceous rocks cropping out in central Chile.

Acknowledgements Funding for this research was provided by the Fondo Nacional de Desarrollo Científico y Tecnológico Grant 1010825 from the Chilean Commission for Scientific and Technological Research. This manuscript was greatly improved by the constructive comments of Dr. Georges Beaudoin, Dr. Slawornir Oszczepalski, Dr. Nicholas Wilson and Dr. Alex Brown.

References

Aberg G, Aguirre L, Levi B, Nystrom O (1984) Spreading subsidence and generation of ensialic marginal basins, an example from the early Cretaceous of Central Chile. In: Kokelaar BP, Howels MF (eds) Marginal basin geology. Geological Society of London, special publication, vol 16. Blackwell Scientific, London, pp 185–193

Arévalo C (1994) Mapa geológico del cuadrángulo Los Loros. Documentos de Trabajo N° 6. SERNAGEOMIN. Scale 1: 100.000

Arévalo C (1995) Mapa geológico de la Hoja Copiapó, Región de Atacama. Documentos de Trabajo N° 6. SERNAGEOMIN. Scale 1:100.000

Arévalo C (1999) The Coastal Cordillera/Precordillera boundary in the Copiapó area, northern Chile and the structural setting of the Candelaria Cu–Au deposit. Ph.D. thesis, University of Kingston, p 205

Barker CE, Pawlewicz MJ (1994) Calculation of vitrinite reflectance from thermal histories and peak temperatures. A comparison of methods. In: Mukhopadhyay PK, Dow WG (eds) Vitrinite reflectance as a maturity parameter: applications and limitations. ACS Symp Ser 570:216–229

Boric R, Holmgren C, Wilson NSF, Zentilli M (2002) The geology of the El Soldado manto-type Cu (Ag) deposit, Central Chile. In: Porter TM (ed) Hydrothermal iron oxide copper–gold and related deposits: a global perspective, vol 2. PGC, Adelaide, pp 163–184

Bustin RM, Cameron A, Grieve D, Kalkreuth W (1985) Coal petrology, its principles and applications. Geological Association of Canada, short course notes, 2nd edn. Geological Association of Canada, St. John's, p 230

Cisternas ME, Diaz L (1990) Geologic evolution of the Atacama basin during the Lower Cretaceous. In: Fontboté L, Amstutz CG, Cardozo M, Cedillo E, Frutos J (eds) Stratabound ore deposits in the Andes. Springer, Berlin Heidelberg New York, pp 496–504

Cisternas ME, Frutos J (1996) Importancia metalogénica del volcanismo extensional del Cretácico Inferior en la Región de Copiapó, Chile. In: XXXIX Congresso Brasileiro de Geologia, vol 7. Anais, Salvador, pp 303–306

Cisternas ME, Frutos J, Spiro B, Galindo E (1999a) Lavas con bitumen en el Cretácico Inferior de Copiapó: petroquímica e importancia metalogénica. Rev Geol Chile 26(2):205–226

Cisternas ME, Haggan T, Parnell J (1999b) Andesita-hosted copper sulphide-bitumen mineralization in a back arc Andean Basin, North Central Chile. In: Stanley CJ et al. (eds) Mineral deposits: processes to processing, vol 1. Balkema, Rotterdam, pp 223–226

Cucurella J, Canut de Bon C, Cisternas ME (2005) Pyrobitumen related to silver–copper deposits in a Cretaceous volcanic–sedimentary sequence: Talcuna district, Coquimbo, Chile. Mineral Pol 36(1):21–29

Davis DW, Lowenstein TK, Spencer RJ (1990) Melting behavior of fluid inclusions in laboratory-grown halite crystal in the system NaCl–H_2O, NaCl–H_2O–KCl, NaCl–H_2O–$MgCl_2$, and NaCl–H_2O–$CaCl_2$. Geochim Cosmochim Acta 54:591–601

Goodarzi F, Gentis T, Jackson G, Macqueen RW (1993) Optical characteristics of head-effected bitumens from the Nanisivik mine, NW Baffin Island, Arctic Canada. Energy Resour 15: 359–376

Haggan T, Parnell J, Cisternas ME (2003) Fluid history of andesite-hosted CuS-bitumen mineralization, Copiapó district, North Central Chile. J Geochem Explor 78–79:631–633

Hermosilla J (2001) Rol de la materia orgánica en la formación de los depósitos minerales del Metalotecto Ocoita-Pabellón. Copiapó, III Región de Atacama. Undergraduate Thesis, Departamento de Ciencias de la Tierra, Universidad de Concepción, p 213

Hoefs J (1987) Stable isotope geochemistry. Springer, Berlin Heidelberg New York, p 236

Hunt JM (1978) Characterization of bitumens and coals. Am Assoc Pet Geol Bull 54:249–273

Jacob H (1989) Classification, structure, genesis and practical importance of natural solid oil bitumen ("migrabitumen"). Int J Coal Geol 11:65–79

Landis CR, Castaño JR (1995) Maturation and bulk chemical properties of a suite of solid hydrocarbons. Org Geochem 22:137–149

Larson R, Pitman WC (1972) World-wide correlation of Mesozoic magnetic anomalies and its applications. GSA Bull 83: 3645–3662

Lewan MD (1983) Effects of thermal maturation on stable carbon isotopes as determined by hydrous pyrolisis of Woodford shale. Geochim Cosmochim Acta 47:1471–1480

Longstaffe FJ, Ayalon A (1987) Oxygen-isotope studies of clastic diagenesis in the Lower Cretaceous Viking Formation, Alberta: implications for the role of meteoric water. In: Marshall JD (ed) Diagenesis of sedimentary sequences. Geological Society, special publication, vol 36. Oxford University Press, Oxford, pp 277–296

Marschik R, Fontboté L (2001) The Punta del Cobre Formation. Punta del Cobre-Candelaria area, northern Chile. J South Am Earth Sci 14:401–433

Marschik R, Fontignie D, Chiaradia M, Voldet P (2003) Geochemical and Sr–Nd–O isotope composition of granitoids of the Early Cretaceous Copiapó plutonic complex (27°30′ S), Chile. J South Am Earth Sci 16:381–398

Mpodozis C, Ramos V (1990) The Andes of Chile and Argentina. Circum Pacific council for energy and minerals resources. Earth Sci Ser 11:59–90

Ohmoto H (1972) Systematics of sulfur and carbon isotopes in hydrothermal ore deposits. Econ Geol 67:551–578

O'Neil JR, Clayton N, Mayeda TK (1969) Oxygen isotope fractionation in divalent metal carbonates. J Chem Phys 51:5547–5558

Potter RW, Clynne MA, Brown DL (1978) Freezing point depression of aqueous sodium solutions. Econ Geol 73:233–244

Rye RO, Ohmoto H (1974) Sulphur and carbon isotopes and ore genesis. A review. Econ Geol 69:826–842

Segerstrom K (1960) Cuadrángulo Quebrada Paipote. Inst Inves Geol Carta Geológica de Chile.Vol.7, N° 1, scale 1:50.000

Segerstrom K (1968) Geología de las hojas Copiapó y Ojos del Salado. Provincia de Atacama. Inst Inv Geol Boletín 24:58

Thomas H (1958) Geología de la Cordillera de la Costa entre el valle de La Ligua y la cuesta Barriga. Ins Inv Geol Boletín 2:86

Ullrich TD, Clark AH, Kyser KT (2001) The Candelaria Cu–Au deposit, III region, Chile: product of long-term mixing of magmatic–hydrothermal and evaporite-source fluids. GSA annual meeting, Boston, 1–10 November 2001

Vaughan APM (1995) Circum-pacific mid-Cretaceous deformation and uplift: a superplume-related event? Geology 23:491–494

Vergara M, Nystrom JO (1996) Geochemical features of Lower Cretaceous backarc lavas in the Andean Cordillera, Central Chile (31–34°S). Rev Geol Chile 23(1):97–106

Wilson NSF (1998) The role of petroleum in the formation of the El Soldado copper deposit, Chile: hydrothermal replacement of a biodegraded petroleum reservoir. Ph.D. Thesis, Dalhousie University, p 418

Wilson NSF (2000) Organic petrology, chemical composition, and reflectance of pyrobitumen from the El Soldado Cu deposit, Chile. Int J Coal Geol 43:53–82

Wilson NSF, Zentilli M (1999) The role of organic matter in the genesis of the El Soldado volcanic-hosted manto-type Cu deposit, Chile. Econ Geol 94:1115–1136

Wilson NSF, Zentilli M, Reynolds PH, Boric R (2003a) $^{40}Ar/^{39}Ar$ geochronology of K-feldspar from the El Soldado manto-type copper deposit, Chile. Chem Geol Isot Geosci Sect 197: 161–176

Wilson NSF, Zentilli M, Spiro B (2003b) A sulfur, carbon, oxygen, and strontium isotope study of the volcanic-hosted El Soldado manto-type copper deposit, Chile: the essential role of bacteria and petroleum. Econ Geol 98(1):163–174

Wilson NSF, Zentilli M (2006) Association of pyrobitumen with copper mineralization from the Uchumi and Talcuna districts, central Chile. Int J Coal Geol 65(1–2):158–169

Zentilli M, Boric R, Munizaga F, Graves MC (1994) Petroleum involvement in the genesis of some strata-bound copper deposits of Chile, VII Congreso Geológico Chileno, vol 2. Concepción pp 1542–1546